

A Search for Excited Neutrinos in e^-p Collisions at HERA

H1 Collaboration

Abstract

A search for excited neutrinos is performed using the full e^-p data sample collected by the H1 experiment at HERA at a centre-of-mass energy of 319 GeV, corresponding to a total luminosity of 184 pb^{-1} . The electroweak decays of excited neutrinos $\nu^* \rightarrow \nu\gamma$, $\nu^* \rightarrow \nu Z$ and $\nu^* \rightarrow eW$ with subsequent hadronic or leptonic decays of the W and Z bosons are considered. No evidence for excited neutrino production is found. Mass dependent exclusion limits on ν^* production cross sections and on the ratio of the coupling to the compositeness scale f/Λ are derived within gauge mediated models. A limit on f/Λ , independent of the relative couplings to the SU(2) and U(1) gauge bosons, is also determined. These limits extend the excluded region to higher masses than has been possible in previous excited neutrino searches.

Submitted to *Phys. Lett. B*

F.D. Aaron^{5,49}, C. Alexa⁵, V. Andreev²⁵, B. Antunovic¹¹, S. Aplin¹¹, A. Asmone³³,
 A. Astvatsatourov⁴, S. Backovic³⁰, A. Baghdasaryan³⁸, P. Baranov^{25,†}, E. Barrelet²⁹,
 W. Bartel¹¹, S. Baudrand²⁷, M. Beckingham¹¹, K. Begzsuren³⁵, O. Behnke¹⁴, A. Belousov²⁵,
 N. Berger⁴⁰, J.C. Bizot²⁷, M.-O. Boenig⁸, V. Boudry²⁸, I. Bozovic-Jelisavcic², J. Bracinik²⁶,
 G. Brandt¹⁴, M. Brinkmann¹¹, V. Brisson²⁷, D. Bruncko¹⁶, A. Bunyatyan^{13,38}, G. Buschhorn²⁶,
 L. Bystritskaya²⁴, A.J. Campbell¹¹, K.B. Cantun Avila²², F. Cassol-Brunner²¹, K. Cerny³²,
 V. Cerny^{16,47}, V. Chekelian²⁶, A. Cholewa¹¹, J.G. Contreras²², J.A. Coughlan⁶, G. Cozzika¹⁰,
 J. Cvach³¹, J.B. Dainton¹⁸, K. Daum^{37,43}, M. Deák¹¹, Y. de Boer²⁴, B. Delcourt²⁷,
 M. Del Degan⁴⁰, J. Delvax⁴, A. De Roeck^{11,45}, E.A. De Wolf⁴, C. Diaconu²¹, V. Dodonov¹³,
 A. Dossanov²⁶, A. Dubak^{30,46}, G. Eckerlin¹¹, V. Efremenko²⁴, S. Egli³⁶, F. Eisele¹⁴,
 A. Eliseev²⁵, E. Elsen¹¹, S. Essenov²⁴, A. Falkiewicz⁷, P.J.W. Faulkner³, L. Favart⁴,
 A. Fedotov²⁴, R. Felst¹¹, J. Feltesse^{10,48}, J. Ferencei¹⁶, L. Finke¹¹, M. Fleischer¹¹,
 A. Fomenko²⁵, G. Franke¹¹, T. Frisson²⁸, E. Gabathuler¹⁸, J. Gayler¹¹, S. Ghazaryan³⁸,
 A. Glazov¹¹, I. Glushkov³⁹, L. Goerlich⁷, M. Goettlich¹², N. Gogitidze²⁵, M. Gouzevitch²⁸,
 C. Grab⁴⁰, T. Greenshaw¹⁸, B.R. Grell¹¹, G. Grindhammer²⁶, S. Habib^{12,50}, D. Haidt¹¹,
 M. Hansson²⁰, C. Helebrant¹¹, R.C.W. Henderson¹⁷, H. Henschel³⁹, G. Herrera²³,
 M. Hildebrandt³⁶, K.H. Hiller³⁹, D. Hoffmann²¹, R. Horisberger³⁶, A. Hovhannisyan³⁸,
 T. Hreus^{4,44}, M. Jacquet²⁷, M.E. Janssen¹¹, X. Janssen⁴, V. Jemanov¹², L. Jönsson²⁰,
 D.P. Johnson^{4,†}, A.W. Jung¹⁵, H. Jung¹¹, M. Kapichine⁹, J. Katzy¹¹, I.R. Kenyon³,
 C. Kiesling²⁶, M. Klein¹⁸, C. Kleinwort¹¹, T. Klimkovich, T. Kluge¹⁸, A. Knutsson¹¹,
 R. Kogler²⁶, V. Korbel¹¹, P. Kostka³⁹, M. Kraemer¹¹, K. Krastev¹¹, J. Kretzschmar³⁹,
 A. Kropivnitskaya²⁴, K. Krüger¹⁵, K. Kutak¹¹, M.P.J. Landon¹⁹, W. Lange³⁹,
 G. Laštovička-Medin³⁰, P. Laycock¹⁸, A. Lebedev²⁵, G. Leibenguth⁴⁰, V. Lendermann¹⁵,
 S. Levonian¹¹, G. Li²⁷, K. Lipka¹², A. Liptaj²⁶, B. List¹², J. List¹¹, N. Loktionova²⁵,
 R. Lopez-Fernandez²³, V. Lubimov²⁴, A.-I. Lucaci-Timoce¹¹, L. Lytkin¹³, A. Makankine⁹,
 E. Malinovski²⁵, P. Marage⁴, Ll. Marti¹¹, H.-U. Martyn¹, S.J. Maxfield¹⁸, A. Mehta¹⁸,
 K. Meier¹⁵, A.B. Meyer¹¹, H. Meyer¹¹, H. Meyer³⁷, J. Meyer¹¹, V. Michels¹¹, S. Mikocki⁷,
 I. Milcewicz-Mika⁷, F. Moreau²⁸, A. Morozov⁹, J.V. Morris⁶, M.U. Mozer⁴, M. Mudrinic²,
 K. Müller⁴¹, P. Murín^{16,44}, K. Nankov³⁴, B. Naroska¹², Th. Naumann³⁹, P.R. Newman³,
 C. Niebuhr¹¹, A. Nikiforov¹¹, G. Nowak⁷, K. Nowak⁴¹, M. Nozicka¹¹, B. Olivier²⁶,
 J.E. Olsson¹¹, S. Osman²⁰, D. Ozerov²⁴, V. Palichik⁹, I. Panagoulis^{1,11,42}, M. Pandurovic²,
 Th. Papadopoulou^{1,11,42}, C. Pascaud²⁷, G.D. Patel¹⁸, O. Pejchal³², H. Peng¹¹, E. Perez^{10,45},
 A. Petrukhin²⁴, I. Picuric³⁰, S. Piec³⁹, D. Pitzl¹¹, R. Plačakyte¹¹, R. Polifka³², B. Povh¹³,
 T. Preda⁵, V. Radescu¹¹, A.J. Rahmat¹⁸, N. Raicevic³⁰, A. Raspiareza²⁶, T. Ravdandorj³⁵,
 P. Reimer³¹, C. Risler¹¹, E. Rizvi¹⁹, P. Robmann⁴¹, B. Roland⁴, R. Roosen⁴, A. Rostovtsev²⁴,
 M. Rotaru⁵, J.E. Ruiz Tabasco²², Z. Rurikova¹¹, S. Rusakov²⁵, D. Salek³², F. Salvaire¹¹,
 D.P.C. Sankey⁶, M. Sauter⁴⁰, E. Sauvan²¹, S. Schmidt¹¹, S. Schmitt¹¹, C. Schmitz⁴¹,
 L. Schoeffel¹⁰, A. Schöning⁴¹, H.-C. Schultz-Coulon¹⁵, F. Sefkow¹¹, R.N. Shaw-West³,
 I. Sheviakov²⁵, L.N. Shtarkov²⁵, T. Sloan¹⁷, I. Smiljanic², P. Smirnov²⁵, Y. Soloviev²⁵,
 D. South⁸, V. Spaskov⁹, A. Specka²⁸, Z. Staykova¹¹, M. Steder¹¹, B. Stella³³, U. Straumann⁴¹,
 D. Sunar⁴, T. Sykora⁴, V. Tchoulakov⁹, G. Thompson¹⁹, P.D. Thompson³, T. Toll¹¹,
 F. Tomasz¹⁶, T.H. Tran²⁷, D. Traynor¹⁹, T.N. Trinh²¹, P. Truöl⁴¹, I. Tsakov³⁴,
 B. Tseepeldorj^{35,51}, I. Tsurin³⁹, J. Turnau⁷, E. Tzamariudaki²⁶, K. Urban¹⁵, A. Valkárová³²,
 C. Vallée²¹, P. Van Mechelen⁴, A. Vargas Trevino¹¹, Y. Vazdik²⁵, S. Vinokurova¹¹,
 V. Volchinski³⁸, D. Wegener⁸, M. Wessels¹¹, Ch. Wissing¹¹, R. Wolf¹⁴, E. Wünsch¹¹,
 V. Yeganov³⁸, J. Žáček³², J. Zálešák³¹, Z. Zhang²⁷, A. Zhelezov²⁴, A. Zhokin²⁴, Y.C. Zhu¹¹,

T. Zimmermann⁴⁰, H. Zohrabyan³⁸, and F. Zomer²⁷

- ¹ *I. Physikalisches Institut der RWTH, Aachen, Germany^a*
- ² *Vinca Institute of Nuclear Sciences, Belgrade, Serbia*
- ³ *School of Physics and Astronomy, University of Birmingham, Birmingham, UK^b*
- ⁴ *Inter-University Institute for High Energies ULB-VUB, Brussels; Universiteit Antwerpen, Antwerpen; Belgium^c*
- ⁵ *National Institute for Physics and Nuclear Engineering (NIPNE) , Bucharest, Romania*
- ⁶ *Rutherford Appleton Laboratory, Chilton, Didcot, UK^b*
- ⁷ *Institute for Nuclear Physics, Cracow, Poland^d*
- ⁸ *Institut für Physik, TU Dortmund, Dortmund, Germany^a*
- ⁹ *Joint Institute for Nuclear Research, Dubna, Russia*
- ¹⁰ *CEA, DSM/DAPNIA, CE-Saclay, Gif-sur-Yvette, France*
- ¹¹ *DESY, Hamburg, Germany*
- ¹² *Institut für Experimentalphysik, Universität Hamburg, Hamburg, Germany^a*
- ¹³ *Max-Planck-Institut für Kernphysik, Heidelberg, Germany*
- ¹⁴ *Physikalisches Institut, Universität Heidelberg, Heidelberg, Germany^a*
- ¹⁵ *Kirchhoff-Institut für Physik, Universität Heidelberg, Heidelberg, Germany^a*
- ¹⁶ *Institute of Experimental Physics, Slovak Academy of Sciences, Košice, Slovak Republic^f*
- ¹⁷ *Department of Physics, University of Lancaster, Lancaster, UK^b*
- ¹⁸ *Department of Physics, University of Liverpool, Liverpool, UK^b*
- ¹⁹ *Queen Mary and Westfield College, London, UK^b*
- ²⁰ *Physics Department, University of Lund, Lund, Sweden^g*
- ²¹ *CPPM, CNRS/IN2P3 - Univ. Mediterranee, Marseille - France*
- ²² *Departamento de Física Aplicada, CINVESTAV, Mérida, Yucatán, México^j*
- ²³ *Departamento de Física, CINVESTAV, México^j*
- ²⁴ *Institute for Theoretical and Experimental Physics, Moscow, Russia*
- ²⁵ *Lebedev Physical Institute, Moscow, Russia^e*
- ²⁶ *Max-Planck-Institut für Physik, München, Germany*
- ²⁷ *LAL, Univ Paris-Sud, CNRS/IN2P3, Orsay, France*
- ²⁸ *LLR, Ecole Polytechnique, IN2P3-CNRS, Palaiseau, France*
- ²⁹ *LPNHE, Universités Paris VI and VII, IN2P3-CNRS, Paris, France*
- ³⁰ *Faculty of Science, University of Montenegro, Podgorica, Montenegro^e*
- ³¹ *Institute of Physics, Academy of Sciences of the Czech Republic, Praha, Czech Republic^h*
- ³² *Faculty of Mathematics and Physics, Charles University, Praha, Czech Republic^h*
- ³³ *Dipartimento di Fisica Università di Roma Tre and INFN Roma 3, Roma, Italy*
- ³⁴ *Institute for Nuclear Research and Nuclear Energy, Sofia, Bulgaria^e*
- ³⁵ *Institute of Physics and Technology of the Mongolian Academy of Sciences , Ulaanbaatar, Mongolia*
- ³⁶ *Paul Scherrer Institut, Villigen, Switzerland*
- ³⁷ *Fachbereich C, Universität Wuppertal, Wuppertal, Germany*
- ³⁸ *Yerevan Physics Institute, Yerevan, Armenia*
- ³⁹ *DESY, Zeuthen, Germany*
- ⁴⁰ *Institut für Teilchenphysik, ETH, Zürich, Switzerlandⁱ*
- ⁴¹ *Physik-Institut der Universität Zürich, Zürich, Switzerlandⁱ*

⁴² Also at Physics Department, National Technical University, Zografou Campus, GR-15773 Athens, Greece

⁴³ Also at Rechenzentrum, Universität Wuppertal, Wuppertal, Germany

⁴⁴ Also at University of P.J. Šafárik, Košice, Slovak Republic

⁴⁵ Also at CERN, Geneva, Switzerland

⁴⁶ Also at Max-Planck-Institut für Physik, München, Germany

⁴⁷ Also at Comenius University, Bratislava, Slovak Republic

⁴⁸ Also at DESY and University Hamburg, Helmholtz Humboldt Research Award

⁴⁹ Also at Faculty of Physics, University of Bucharest, Bucharest, Romania

⁵⁰ Supported by a scholarship of the World Laboratory Björn Wiik Research Project

⁵¹ Also at Ulaanbaatar University, Ulaanbaatar, Mongolia

† Deceased

^a Supported by the Bundesministerium für Bildung und Forschung, FRG, under contract numbers 05 H1 1GUA /1, 05 H1 1PAA /1, 05 H1 1PAB /9, 05 H1 1PEA /6, 05 H1 1VHA /7 and 05 H1 1VHB /5

^b Supported by the UK Particle Physics and Astronomy Research Council, and formerly by the UK Science and Engineering Research Council

^c Supported by FNRS-FWO-Vlaanderen, IISN-IIKW and IWT and by Interuniversity Attraction Poles Programme, Belgian Science Policy

^d Partially Supported by Polish Ministry of Science and Higher Education, grant PBS/DESY/70/2006

^e Supported by the Deutsche Forschungsgemeinschaft

^f Supported by VEGA SR grant no. 2/7062/ 27

^g Supported by the Swedish Natural Science Research Council

^h Supported by the Ministry of Education of the Czech Republic under the projects LC527 and INGO-1P05LA259

ⁱ Supported by the Swiss National Science Foundation

^j Supported by CONACYT, México, grant 48778-F

^l This project is co-funded by the European Social Fund (75%) and National Resources (25%) - (EPEAEK II) - PYTHAGORAS II

1 Introduction

The three-family structure and mass hierarchy of the known fermions is one of the most puzzling characteristics of the Standard Model (SM) of particle physics. Attractive explanations are provided by models assuming composite quarks and leptons [1]. The existence of excited states of leptons and quarks is a natural consequence of these models and their discovery would provide convincing evidence of a new scale of matter. Electron-proton interactions at very high energies provide a good environment in which to search for excited states of first generation fermions. In particular, excited neutrinos (ν^*) could be singly produced through the exchange of a W boson in the t -channel.

In this letter a search for excited neutrinos using the complete e^-p HERA collider data of the H1 experiment is presented. Electroweak decays into a SM lepton (e, ν_e) and a SM gauge boson (γ, W and Z) are considered and hadronic as well as leptonic decays of the W and Z are analysed.

The data, collected at electron and proton beam energies of 27.6 GeV and 920 GeV, respectively, correspond to a total integrated luminosity of 184 pb^{-1} . During the HERA II running period, the electron beam was longitudinally polarised, at a level of typically 35%. For this analysis the periods with left-handed and right-handed beams are combined and the analysed data sample has a residual polarisation of 5% left-handed. With more than a ten-fold increase in statistics, this analysis supersedes the result of the previous H1 search for excited neutrinos based on a data sample corresponding to a luminosity of 15 pb^{-1} [2].

2 Phenomenology

In the present study a model [3–5] is considered in which excited fermions are assumed to have spin $1/2$ and isospin $1/2$. Both left-handed and right-handed components of the excited fermions form weak iso-doublets F_L^* and F_R^* . In order to prevent the light leptons from radiatively acquiring a large anomalous magnetic moment [6, 7], only the right-handed component of the excited fermions takes part in the generalised magnetic de-excitation. The interaction between excited fermions, gauge bosons and ordinary fermions is then described by the effective Lagrangian [4]:

$$\mathcal{L}_{int.} = \frac{1}{2\Lambda} \bar{F}_R^* \sigma^{\mu\nu} \left[g f \frac{\tau^a}{2} W_{\mu\nu}^a + g' f' \frac{Y}{2} B_{\mu\nu} + g_s f_s \frac{\lambda^a}{2} G_{\mu\nu}^a \right] F_L + h.c. . \quad (1)$$

The matrix $\sigma^{\mu\nu}$ is the covariant bilinear tensor, $W_{\mu\nu}^a$, $B_{\mu\nu}$ and $G_{\mu\nu}^a$ are the field-strength tensors of the SU(2), U(1) and SU(3)_C gauge fields, τ^a , Y and λ^a are the Pauli matrices, the weak hypercharge operator and the Gell-Mann matrices, respectively. The standard electroweak and strong gauge couplings are denoted by g , g' and g_s , respectively. The parameter Λ has units of energy and can be regarded as the compositeness scale which reflects the range of a new confinement force. The constants f , f' and f_s are form factors associated to the three gauge groups. They can be interpreted as parameters setting different scales $\Lambda_i = \Lambda/f_i$ for the

different gauge groups, thus allowing the composite fermion to have arbitrary coupling strengths with the three gauge bosons.

Following this model, single production of excited neutrinos in ep collisions may result from the t -channel exchange of a W boson. Due to the helicity dependence of the weak interaction and given the valence quark composition and density distribution of the proton, the ν^* production cross section is predicted to be much larger for e^-p collisions than for e^+p . For a ν^* mass M_{ν^*} of 200 GeV the ratio of the production cross sections is of order 100. The ν^* production cross section is expected to scale linearly with the polarisation of the incident electron beam, similarly to the SM charged current process. The excited neutrino may decay into a lepton and an electroweak gauge boson via $\nu^* \rightarrow \nu\gamma$, $\nu^* \rightarrow eW$ and $\nu^* \rightarrow \nu Z$. For a given M_{ν^*} value and assuming a numerical relation between f and f' , the ν^* branching ratios are fixed and the production cross section depends only on f/Λ . The ν^* is expected not to have strong interactions and therefore this search is insensitive to f_s . Two complementary coupling assignments $f = +f'$ and $f = -f'$ are studied in detail. For $f = +f'$ the excited neutrino has no tree-level electromagnetic coupling [8] and therefore the photonic decay of the ν^* is forbidden whereas for $f = -f'$ decays into $\nu\gamma$, νZ and eW are allowed. In addition, arbitrary ratios of f'/f are considered in the range -5 to $+5$.

3 Simulation of Signal and Background Processes

A Monte Carlo (MC) program developed for this analysis is used for the calculation of the ν^* production cross section and the simulation of signal events. The events are simulated using the cross section calculated from the Lagrangian described in equation (1) using the CompHEP package [9]. Initial state radiation from the incident electron is included using the Weizsäcker-Williams approximation [10]. The proton parton densities are taken from the CTEQ5L [11] parametrisation and are evaluated at the scale $\sqrt{Q^2}$, where Q^2 is the four-momentum transfer squared. The parton shower approach [12] is applied to simulate Quantum Chromodynamics (QCD) corrections in the initial and final states. The hadronisation is performed using Lund string fragmentation as implemented in PYTHIA [12].

In the MC generator the full transition matrix including the production and the decay is implemented. This is important if the natural width of the ν^* is large, which is typically the case at high mass where factorisation of the ν^* production and its decay no longer holds. Events used in the determination of signal efficiencies are generated with the coupling f/Λ corresponding, for each ν^* mass, to the expected boundary of the probed domain in the plane defined by M_{ν^*} and f/Λ .

The Standard Model background processes that may mimic a ν^* signal are neutral current (NC) and charged current (CC) deep-inelastic scattering (DIS) and to a lesser extent photoproduction, lepton pair production and real W boson production.

The RAPGAP [13] event generator, which implements the Born, QCD Compton and Boson Gluon Fusion matrix elements, is used to model NC DIS events. The QED radiative effects arising from real photon emission from both the incoming and outgoing electrons are simulated using the HERACLES [14] program. Direct and resolved photoproduction of jets and prompt

photon production are simulated using the PYTHIA event generator. The simulation is based on Born level hard scattering matrix elements with radiative QED corrections. In RAPGAP and PYTHIA, jet production from higher order QCD radiation is simulated using leading logarithmic parton showers and hadronisation is modelled with Lund string fragmentation. The leading order MC prediction of NC DIS and photoproduction processes with two or more high transverse momentum jets is scaled by a factor of 1.2 in order to normalise to next-to-leading order QCD calculations [15]. Charged current DIS events are simulated using the DJANGO [16] program, which includes first order leptonic QED radiative corrections based on HERACLES. The production of two or more jets in DJANGO is accounted for using the colour-dipole-model [17].

Contributions from elastic and quasi-elastic QED Compton scattering are simulated with the WABGEN [18] generator. Contributions arising from the production of W bosons and multi-lepton events are modelled using the EPVEC [19] and GRAPE [20] event generators, respectively.

All processes are generated with an integrated luminosity significantly higher than that of the data sample. Generated events are passed through the full GEANT [21] based simulation of the H1 apparatus, which takes into account the running conditions of the different data taking periods, and are reconstructed and analysed using the same program chain as for the data.

4 Experimental Conditions

A detailed description of the H1 experiment can be found in [22]. Only the detector components relevant to the present analysis are briefly described here. The origin of the H1 coordinate system is the nominal ep interaction point, with the direction of the proton beam defining the positive z -axis (forward region). Transverse momentum (P_T) is measured in the xy plane. The pseudorapidity η is related to the polar angle θ by $\eta = -\ln \tan(\theta/2)$. The Liquid Argon (LAr) calorimeter [23] is used to measure electrons, photons and hadrons. It covers the polar angle range $4^\circ < \theta < 154^\circ$ with full azimuthal acceptance. Electromagnetic shower energies are measured with a precision of $\sigma(E)/E = 12\%/\sqrt{E/\text{GeV}} \oplus 1\%$ and hadronic energies with $\sigma(E)/E = 50\%/\sqrt{E/\text{GeV}} \oplus 2\%$, as measured in test beams [24, 25]. In the backward region, energy measurements are provided by a lead/scintillating-fiber (SpaCal) calorimeter [26] covering the angular range $155^\circ < \theta < 178^\circ$. The central ($20^\circ < \theta < 160^\circ$) and forward ($7^\circ < \theta < 25^\circ$) tracking detectors are used to measure charged particle trajectories, to reconstruct the interaction vertex and to complement the measurement of hadronic energy. The LAr and inner tracking detectors are enclosed in a super-conducting magnetic coil with a field strength of 1.16 T. The return yoke of the coil is the outermost part of the detector and is equipped with streamer tubes forming the central muon detector ($4^\circ < \theta < 171^\circ$). In the forward region of the detector ($3^\circ < \theta < 17^\circ$) a set of drift chambers detects muons and measures their momenta using an iron toroidal magnet. The luminosity is determined from the rate of the Bethe-Heitler process $ep \rightarrow ep\gamma$, measured using a photon detector located close to the beam pipe at $z = -103$ m, in the backward direction.

5 Data Analysis

The triggers used in this analysis are based on the detection of energy deposits in the LAr calorimeter [27]. Events containing an electromagnetic deposit (electron or photon) with an energy greater than 10 GeV are triggered with an efficiency close to 100%. For events with missing transverse energy above 20 GeV, the trigger efficiency is $\sim 90\%$.

In order to remove background events induced by cosmic showers and other non- ep sources, the event vertex is required to be reconstructed within 35 cm in z of the nominal interaction point. In addition, topological filters and timing vetoes are applied.

The identification of electrons or photons relies on the measurement of a compact and isolated electromagnetic shower in the LAr calorimeter. In addition, the hadronic energy within a distance in the pseudorapidity-azimuth ($\eta - \phi$) plane $R = \sqrt{\Delta\eta^2 + \Delta\phi^2} < 0.5$ around the electron (photon) is required to be below 3% of the electron (photon) energy. Muon identification is based on a track measured in the inner tracking systems associated with signals in the muon detectors [28]. A muon candidate should have no more than 5 GeV deposited in a cylinder, centred on the muon track direction, of radius 25 cm and 50 cm in the electromagnetic and hadronic sections of the LAr calorimeter, respectively. Calorimeter energy deposits and tracks not previously identified as electron, photon or muon candidates are used to form combined cluster-track objects, from which the hadronic energy is reconstructed [29, 30]. Jets are reconstructed from these combined cluster-track objects using an inclusive k_T algorithm [31, 32] with a minimum transverse momentum of 2.5 GeV. The missing transverse momentum P_T^{miss} of the event is derived from all identified particles and energy deposits in the event. The P_T^{miss} is assumed to originate from a single neutrino. The four-vector of this neutrino candidate is reconstructed assuming transverse momentum conservation and the relation $\sum_i (E^i - P_z^i) + (E^\nu - P_z^\nu) = 2E_e^0 = 55.2 \text{ GeV}$, where the sum runs over all detected particles; P_z is the momentum along the beam axis and E_e^0 is the electron beam energy.

Specific selection criteria applied in each decay channel are presented in the following subsections. A detailed description of the analysis can be found in [33].

5.1 $\nu\gamma$ Resonance Search

The signature of the decay channel $\nu^* \rightarrow \nu\gamma$ consists of an isolated electromagnetic cluster in events with missing transverse momentum. Background arises from CC DIS events with an isolated π^0 or a radiated photon. Events with substantial missing transverse momentum $P_T^{\text{miss}} > 20 \text{ GeV}$ are selected. In each event, a photon candidate with transverse momentum $P_T^\gamma > 20 \text{ GeV}$ in a polar angle range $5^\circ < \theta^\gamma < 120^\circ$ is required. This polar angle range is restricted to $\theta^\gamma < 60^\circ$ in events with P_T^{miss} below 30 GeV, in order to reduce background from NC DIS. The photon is required to be isolated from jets by a distance $R > 0.5$ to any jet axis. In the central region ($\theta^\gamma > 20^\circ$), photon candidates are selected only if no well measured track points to the electromagnetic cluster within a distance of closest approach (DCA) of 12 cm. For events with P_T^{miss} below 50 GeV, this condition is tightened by accepting only photon candidates having no track with a DCA to the cluster below 24 cm or within $R < 0.5$. The energy and polar angle of the photon are combined into one discriminant variable $\xi^\gamma = E^\gamma \cos^2(\theta^\gamma/2)$.

Radiative CC DIS events are suppressed by requiring that $\xi^\gamma > 45$ GeV. For signal events, in most cases the final state contains a recoil jet, due to ν^* production via t -channel W boson exchange. Hence, in the final selection the presence of at least one jet with $P_T^{\text{jet}} > 5$ GeV is also required.

Seven events are selected in the data, compared to a SM expectation of 12.3 ± 3.0 , which is dominated by CC DIS events. The invariant mass of the excited neutrino candidate is calculated from the four-vectors of the neutrino and the photon. The invariant mass distributions of the ν^* candidates and of the expected SM background are presented in figure 1(a). The resulting selection efficiency is 50% for $M_{\nu^*} = 120$ GeV, increasing to 55% for $M_{\nu^*} = 260$ GeV. From Monte Carlo studies, the total width of the reconstructed ν^* mass distribution is 11 GeV for a generated ν^* mass of 120 GeV, increasing to 41 GeV for a ν^* mass of 260 GeV.

5.2 $\nu q\bar{q}$ Resonance Search

The signature of the $\nu^* \rightarrow \nu Z \rightarrow \nu q\bar{q}$ decay channel consists of two jets with high transverse momentum in events with large P_T^{miss} . The SM background is dominated by multi-jet CC DIS events and contains a moderate contribution from photoproduction. Events with missing transverse momentum $P_T^{\text{miss}} > 20$ GeV are selected. In each event at least two jets are required in the polar angle range $5^\circ < \theta^{\text{jet}} < 130^\circ$ with transverse momenta larger than 20 and 15 GeV, respectively. Additionally, the hadronic final state must exhibit a polar angle γ_h , as defined in [34], larger than 20° , in order to remove photoproduction events. Events with $P_T^{\text{miss}} < 30$ GeV are selected if the ratio V_{ap}/V_p of transverse energy flow anti-parallel and parallel to the hadronic final state [34] is above 0.1. This condition reduces the contribution of CC DIS processes. Photoproduction and NC DIS backgrounds typically have low values of x_h , the Bjorken scaling variable calculated from the hadronic system using the Jacquet-Blondel method [34, 35], and are thus suppressed by requiring $x_h > 0.04$. Finally, to further reduce the background from CC DIS, a jet multiplicity greater than or equal to three is required for events with $P_T^{\text{miss}} < 50$ GeV. In each event, a Z candidate is reconstructed from the combination of the two jets with an invariant mass closest to the nominal Z boson mass. The reconstructed Z candidate is required to have an invariant mass above 60 GeV.

After this selection, 89 events are found in the data compared to a SM expectation of 95 ± 21 events. The invariant mass of the ν^* candidate is calculated from the neutrino and Z candidate four-vectors. For this calculation, the Z candidate four-vector is scaled such that its mass is set equal to the nominal Z boson mass. The invariant mass distributions of the ν^* candidates and of the expected SM background are presented in figure 1(b). The selection efficiency in this channel is 25% for $M_{\nu^*} = 120$ GeV, increasing to 55% for $M_{\nu^*} = 260$ GeV. From Monte Carlo studies, the total width of the reconstructed ν^* mass distribution is 31 GeV for a generated ν^* mass of 120 GeV, increasing to 41 GeV for a ν^* mass of 260 GeV.

5.3 $e q\bar{q}$ Resonance Search

The signature of the $\nu^* \rightarrow e W \rightarrow e q\bar{q}$ decay channel consists of one electron and two high P_T jets. Multi-jet NC DIS events constitute the main background contribution from SM processes.

Events are selected with an isolated electron in the LAr calorimeter in the polar angle range $5^\circ < \theta^e < 90^\circ$. The electron variable¹ $\xi^e = E^e \cos^2(\theta^e/2)$ is required to be above 23 GeV or the electron should have a transverse momentum P_T^e greater than 25 GeV. These conditions remove a large part of the NC DIS contribution. In addition, the electron should be isolated from jets by a distance $R > 0.5$ to any jet axis. The events are required to have at least two jets in the polar angle range $5^\circ < \theta^{\text{jet}} < 130^\circ$ with transverse momenta larger than 20 and 15 GeV, respectively. In each event, a W candidate is reconstructed from the combination of the two jets with an invariant mass closest to the nominal W boson mass. The reconstructed mass of the W candidate is required to be larger than 40 GeV. To further reduce the NC DIS background it is required that the polar angle of the jet with the highest P_T associated to the W candidate be less than 80° and that events with $P_T^e < 65$ GeV contain at least three jets with a P_T larger than 5 GeV.

After the selection, 220 events are observed compared to a SM expectation of 223 ± 47 . The invariant mass of the ν^* candidate is calculated from the electron and W candidate four-vectors. For this calculation, the W candidate four-vector is scaled such that its mass is set equal to the nominal W boson mass. The invariant mass distributions of the ν^* candidates and of the expected SM background are presented in figure 1(c). The selection efficiency in this channel is 40% for $M_{\nu^*} = 120$ GeV, increasing to 65% for $M_{\nu^*} = 260$ GeV. From Monte Carlo studies, the total width of the reconstructed ν^* mass distribution is 15 GeV for a generated ν^* mass of 120 GeV, increasing to 38 GeV for a ν^* mass of 260 GeV.

5.4 $e\nu\mu$ and $e\nu e$ Resonance Searches

In the search for $\nu^* \rightarrow eW \rightarrow e\nu\mu$, events with $P_T^{\text{miss}} > 15$ GeV, one electron with $P_T^e > 20$ GeV and one muon with $P_T^\mu > 10$ GeV are selected. The electron and the muon have to be detected in the polar angle ranges $5^\circ < \theta^e < 100^\circ$ and $10^\circ < \theta^\mu < 160^\circ$, respectively. Furthermore, the electron and the muon must be isolated from jets by minimum distances of $R^e > 0.5$ and $R^\mu > 1$, respectively. The contribution from NC DIS processes is reduced by requiring $\xi^e > 9$ GeV. After this selection no data event remains, while 0.40 ± 0.05 SM background events are expected. The selection efficiency for ν^* with masses above 120 GeV is $\sim 35\%$.

The signatures of the $\nu^* \rightarrow eW \rightarrow e\nu e$ and $\nu^* \rightarrow \nu Z \rightarrow \nu e e$ channels are similar and consist of two high P_T electrons in events with large missing transverse momentum. Events with $P_T^{\text{miss}} > 20$ GeV are selected. In each event two isolated electromagnetic clusters are required, with a transverse momentum larger than 20 and 15 GeV, respectively. The highest P_T electron should be detected in the polar angle range $5^\circ < \theta^{e1} < 100^\circ$ and the second electron in the range $5^\circ < \theta^{e2} < 120^\circ$. To reduce the background from Compton processes, a track has to be associated to each electromagnetic cluster in the central region ($\theta^e > 35^\circ$). Events in which the invariant mass of the two electromagnetic clusters is within 10 GeV of the nominal Z boson mass are attributed to the $Z \rightarrow ee$ decay channel. Events from the $W \rightarrow \nu e$ decay channel are selected by requiring the invariant mass of the ν and one of the electromagnetic clusters to be compatible with the W boson mass within 20 GeV. In this channel, the variable ξ^e defined from the highest P_T electron is required to be above 29 GeV. No data candidate is observed in

¹ This variable is proportional to the four-momentum transfer squared Q^2 for NC DIS.

either the Z or W decay channels compared to SM expectations of 0.19 ± 0.05 and 0.7 ± 0.1 , respectively. In both channels, the selection efficiency for ν^* with masses above 120 GeV is $\sim 35\%$.

5.5 Systematic Uncertainties

The following experimental systematic uncertainties are considered:

- The uncertainty on the electromagnetic energy scale varies between 1% and 3% depending on the polar angle. The polar angle measurement uncertainty of electromagnetic clusters is 3 mrad.
- The efficiency to identify photons is known with a precision of 10% for high P_T photons.
- The scale uncertainty on the transverse momentum of high P_T muons amounts to 5%. The uncertainty on the reconstruction of the muon polar angle is 3 mrad.
- The hadronic energy scale is known within 2%. The uncertainty on the jet polar angle determination is 10 mrad.
- The uncertainty on the trigger efficiency is 3%.
- The luminosity measurement has an uncertainty of 2.5%.

The effect of the above systematic uncertainties are determined by varying the experimental quantities by ± 1 standard deviation in the MC samples and propagating these variations through the whole analysis chain.

Additional model systematic uncertainties are attributed to the SM background MC generators described in section 3. An error of 20% on the simulation of NC DIS, CC DIS and photoproduction processes with at least two high P_T jets is considered to account for the uncertainty on higher order QCD corrections. An uncertainty of 30% on the simulation of radiative CC DIS events is considered to account for the lack of QED radiation from the quark line in the DJANGO generator. This uncertainty is estimated in the specific phase space of the analysis by a comparison of the DJANGO result to the calculated cross section of the $e^-p \rightarrow \nu_e \gamma X$ process [36]. The error on the QED Compton cross section is estimated to be 10%. The errors attributed to multi-lepton and W production are 3% and 15%, respectively. The total error on the SM background prediction is determined by adding the effects of all model and experimental systematic uncertainties in quadrature.

The theoretical uncertainty on the ν^* production cross section is dominated by the uncertainty on the scale at which the proton parton densities are evaluated. It is estimated by varying this scale from $\sqrt{Q^2}/2$ to $2\sqrt{Q^2}$. The resulting uncertainty depends on the ν^* mass and is 10% at $M_{\nu^*} = 100$ GeV, increasing to 30% at $M_{\nu^*} = 300$ GeV.

6 Interpretation

The event yields observed in all decay channels are in agreement with the corresponding SM expectations and are summarised in table 1. The SM predictions are dominated by NC DIS processes for the $eq\bar{q}$ resonance search and by CC DIS for the $\nu\gamma$ and $\nu q\bar{q}$ resonance searches. The distributions of the invariant mass of the data events are in agreement with those of the expected SM background as shown in figure 1. No data event is observed in channels corresponding to leptonic decays of the W or Z bosons, in agreement with the low SM expectations.

Since no evidence for the production of excited neutrinos is observed, upper limits on the ν^* production cross section and on the coupling f/Λ are derived as a function of the mass of the excited neutrino. Limits are presented at the 95% confidence level (CL) and are obtained from the mass spectra using a modified frequentist approach which takes statistical and systematic uncertainties into account [37].

Upper limits on the product of the ν^* production cross section and decay branching ratio are shown in figure 2. The analysed decay channels of the W and Z gauge bosons are combined. The resulting limits on f/Λ after combination of all ν^* decay channels are displayed as a function of the ν^* mass in figure 3, for the conventional assumptions $f = -f'$ and $f = +f'$. Limits are derived for ν^* masses up to 300 GeV. The total fraction of ν^* decays covered in this analysis is $\sim 92\%$ and $\sim 84\%$ in the two cases $f = -f'$ and $f = +f'$, respectively. In the case $f = -f'$, the limit on f/Λ is dominated at low mass by the $\nu^* \rightarrow \nu\gamma$ channel, while the $\nu^* \rightarrow eW$ channel starts to contribute significantly for masses above 200 GeV. Under the assumption $f = +f'$, the limit on f/Λ is driven mainly by the $\nu^* \rightarrow eW$ channel. These new results improve significantly the previously published limits by H1 [2] and ZEUS [38]. For comparison, the most stringent limits obtained in e^+e^- collisions at LEP for the two cases $f = -f'$ and $f = +f'$, determined by L3 [39] and DELPHI [40], respectively, are also shown in figure 3. The H1 measurement provides the most stringent constraints for masses larger than ~ 170 GeV. With the assumption $f/\Lambda = 1/M_{\nu^*}$ excited neutrinos with masses up to 213 GeV (196 GeV) are excluded for $f = -f'$ ($f = +f'$).

Limits with less model dependence can be derived if arbitrary ratios f'/f are considered. The dependence of the limits on this ratio for different ν^* masses is displayed in figure 4(a). Limits which are independent of f'/f are derived for $f'/f \in [-5; 5]$ by choosing in figure 4(a) the point with the weakest limit for each mass hypothesis. The result is shown in figure 4(b) and is found to be almost equal to the limit obtained under the assumption $f = +f'$.

7 Conclusion

Using the full e^-p data sample collected by the H1 experiment at HERA with an integrated luminosity of 184 pb^{-1} a search for the production of excited neutrinos is performed. The excited neutrino decay channels $\nu^* \rightarrow \nu\gamma$, $\nu^* \rightarrow \nu Z$ and $\nu^* \rightarrow eW$ with subsequent hadronic or leptonic decays of the W and Z bosons are considered and no indication of a ν^* signal is found. New limits on the production cross section of excited neutrinos are obtained. Previous HERA results are improved by a factor three to four. Upper limits on the coupling f/Λ as a function of

the excited neutrino mass are established for specific relations between the couplings ($f = +f'$ and $f = -f'$) and independent of the ratio f'/f . Assuming $f = -f'$ and $f/\Lambda = 1/M_{\nu^*}$, excited neutrinos with a mass lower than 213 GeV are excluded at 95% confidence level. The results presented in this letter greatly extend the previously excluded domain and demonstrate the unique sensitivity of HERA to excited neutrinos with masses beyond the LEP reach.

Acknowledgements

We are grateful to the HERA machine group whose outstanding efforts have made this experiment possible. We thank the engineers and technicians for their work in constructing and maintaining the H1 detector, our funding agencies for financial support, the DESY technical staff for continual assistance and the DESY directorate for the hospitality which they extend to the non DESY members of the collaboration. We would like to thank M. Spira for helpful discussions.

References

- [1] H. Harari, Phys. Rept. **104** (1984) 159.
- [2] C. Adloff *et al.* [H1 Collaboration], Phys. Lett. B **525** (2002) 9 [hep-ex/0110037].
- [3] K. Hagiwara, D. Zeppenfeld and S. Komamiya, Z. Phys. C **29** (1985) 115.
- [4] F. Boudjema, A. Djouadi and J. L. Kneur, Z. Phys. C **57** (1993) 425.
- [5] U. Baur, M. Spira and P. M. Zerwas, Phys. Rev. D **42** (1990) 815.
- [6] S. J. Brodsky and S. D. Drell, Phys. Rev. D **22** (1980) 2236.
- [7] F. M. Renard, Phys. Lett. B **116** (1982) 264.
- [8] F. Boudjema and A. Djouadi, Phys. Lett. B **240** (1990) 485.
- [9] E. Boos *et al.* [CompHEP Collaboration], Nucl. Instrum. Meth. A **534** (2004) 250 [hep-ph/0403113];
A. Pukhov *et al.*, “CompHEP - a package for evaluation of Feynman diagrams and integration over multi-particle phase space”, hep-ph/9908288
(available at <http://theory.sinp.msu.ru/comphep>).
- [10] C. Berger and W. Wagner, Phys. Rept. **146** (1987) 1.
- [11] J. Pumplin *et al.*, JHEP **0207** (2002) 012 [hep-ph/0201195].
- [12] T. Sjöstrand *et al.*, PYTHIA version 6.1, Comput. Phys. Commun. **135** (2001) 238 [hep-ph/0010017].
- [13] H. Jung, RAPGAP version 3.1, Comput. Phys. Commun. **86** (1995) 147.

- [14] A. Kwiatkowski, H. Spiesberger and H. J. Möhring, *Comput. Phys. Commun.* **69** (1992) 155.
- [15] C. Adloff *et al.* [H1 Collaboration], *Eur. Phys. J. C* **25** (2002) 13 [hep-ex/0201006].
- [16] G. A. Schuler and H. Spiesberger, DJANGO version 1.4, “Django: The Interface for The Event Generators Heracles and Lepto”, *Proc. of the Workshop “Physics at HERA”* (1991), Eds. W. Buchmüller and G. Ingelman, Vol. 3, p. 1419.
- [17] L. Lönnblad, *Comput. Phys. Commun.* **71** (1992) 15.
- [18] C. Berger and P. Kandel, “A New Generator For Wide Angle Bremsstrahlung”, Prepared for Workshop on Monte Carlo Generators for HERA Physics Hamburg, Germany, 27-30 April 1998.
- [19] U. Baur, J. A. Vermaseren and D. Zeppenfeld, EPVEC version 1.1, *Nucl. Phys. B* **375** (1992) 3.
- [20] T. Abe, GRAPE-Dilepton version 1.1, *Comput. Phys. Commun.* **136** (2001) 126 [hep-ph/0012029].
- [21] R. Brun *et al.*, “Geant3”, CERN-DD/EE/84-1.
- [22] I. Abt *et al.* [H1 Collaboration], *Nucl. Instrum. Meth. A* **386** (1997) 310;
I. Abt *et al.* [H1 Collaboration], *Nucl. Instrum. Meth. A* **386** (1997) 348.
- [23] B. Andrieu *et al.* [H1 Calorimeter Group Collaboration], *Nucl. Instrum. Meth. A* **336** (1993) 460.
- [24] B. Andrieu *et al.* [H1 Calorimeter Group Collaboration], *Nucl. Instrum. Meth. A* **336** (1993) 499.
- [25] B. Andrieu *et al.* [H1 Calorimeter Group Collaboration], *Nucl. Instrum. Meth. A* **350** (1994) 57.
- [26] R. D. Appuhn *et al.* [H1 SPACAL Group Collaboration], *Nucl. Instrum. Meth. A* **386** (1997) 397.
- [27] C. Adloff *et al.* [H1 Collaboration], *Eur. Phys. J. C* **30** (2003) 1 [hep-ex/0304003].
- [28] V. Andreev *et al.* [H1 Collaboration], *Phys. Lett. B* **561** (2003) 241 [hep-ex/0301030].
- [29] M. Peez, “Recherche de déviations au Modèle Standard dans les processus de grande énergie transverse sur le collisionneur électron - proton HERA”, Ph.D. thesis, Université de Lyon (2003), DESY-THESIS-2003-023 (available at <http://www-h1.desy.de/psfiles/theses/>).
- [30] B. Pothault, “Première mesure des sections efficaces de courant chargé et neutre avec le faisceau de positrons polarisé à HERA II et analyses QCD-électrofaibles”, Ph.D. thesis, Université Paris XI (2005), LAL-05-05 (available at <http://www-h1.desy.de/psfiles/theses/>).

- [31] S. D. Ellis and D. E. Soper, Phys. Rev. D **48** (1993) 3160 [hep-ph/9305266].
- [32] S. Catani *et al.*, Nucl. Phys. B **406** (1993) 187.
- [33] T. N. Trinh, “Recherche de leptons excités sur le collisionneur HERA avec le détecteur H1”, Ph.D. thesis, Université de la Méditerranée Aix-Marseille II (2008)
(in preparation, to appear at <http://www-h1.desy.de/psfiles/theses/>).
- [34] C. Adloff *et al.* [H1 Collaboration], Eur. Phys. J. C **13** (2000) 609 [hep-ex/9908059].
- [35] A. Blondel, F. Jacquet, Proceedings of the Study of an ep Facility for Europe, ed. U. Amaldi, DESY 79/48 (1979) 391.
- [36] T. Helbig and H. Spiesberger, Nucl. Phys. B **373** (1992) 73.
- [37] T. Junk, Nucl. Instrum. Meth. A **434** (1999) 435 [hep-ex/9902006].
- [38] S. Chekanov *et al.* [ZEUS Collaboration], Phys. Lett. B **549** (2002) 32 [hep-ex/0109018].
- [39] P. Achard *et al.* [L3 Collaboration], Phys. Lett. B **568** (2003) 23 [hep-ex/0306016].
- [40] J. Abdallah *et al.* [DELPHI Collaboration], Eur. Phys. J. C **46** (2006) 277 [hep-ex/0603045].

Search for ν^* at HERA (e^-p, 184 pb$^{-1}$)			
Channel	Data	SM	Signal Efficiency [%]
$\nu^* \rightarrow \nu\gamma$	7	12.3 ± 3.0	50–55
$\nu^* \rightarrow eW \rightarrow eq\bar{q}$	220	223 ± 47	40–65
$\nu^* \rightarrow eW \rightarrow e\nu\mu$	0	0.40 ± 0.05	35
$\nu^* \rightarrow eW \rightarrow e\nu e$	0	0.7 ± 0.1	45
$\nu^* \rightarrow \nu Z \rightarrow \nu q\bar{q}$	89	95 ± 21	25–55
$\nu^* \rightarrow \nu Z \rightarrow \nu ee$	0	0.19 ± 0.05	45

Table 1: Observed and predicted event yields for the studied ν^* decay channels. The analysed data sample corresponds to an integrated luminosity of 184 pb $^{-1}$. The error on the SM predictions includes model and experimental systematic errors added in quadrature. Typical selection efficiencies for ν^* masses ranging from 120 to 260 GeV are also indicated.

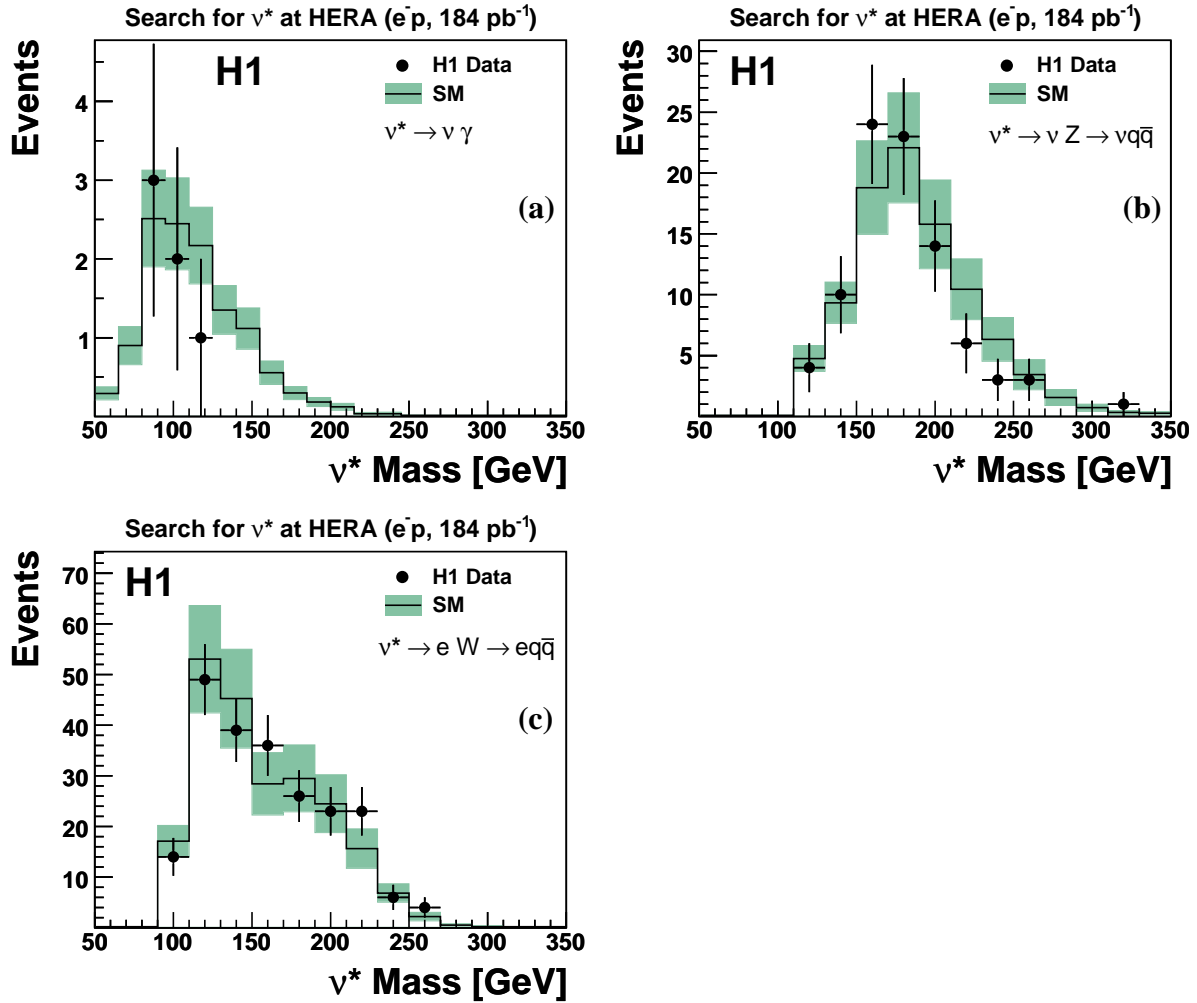


Figure 1: Invariant mass distribution of the ν^* candidates for the $\nu^* \rightarrow \nu \gamma$ (a), $\nu^* \rightarrow \nu Z \rightarrow \nu q \bar{q}$ (b) and $\nu^* \rightarrow e W \rightarrow e q \bar{q}$ (c) searches. The points correspond to the observed data events and the histogram to the SM expectation after the final selections. The error bands on the SM prediction include model and experimental systematic errors added in quadrature.

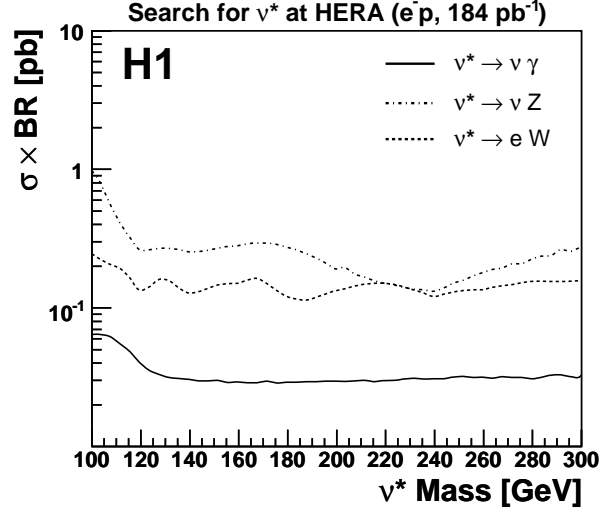


Figure 2: Upper limits at 95% CL on the product of the ν^* production cross section and decay branching ratio, $\sigma \times \text{BR}$, in the three decay channels as a function of the excited neutrino mass. The different decay channels of the W and Z gauge bosons are combined. Areas above the curves are excluded.

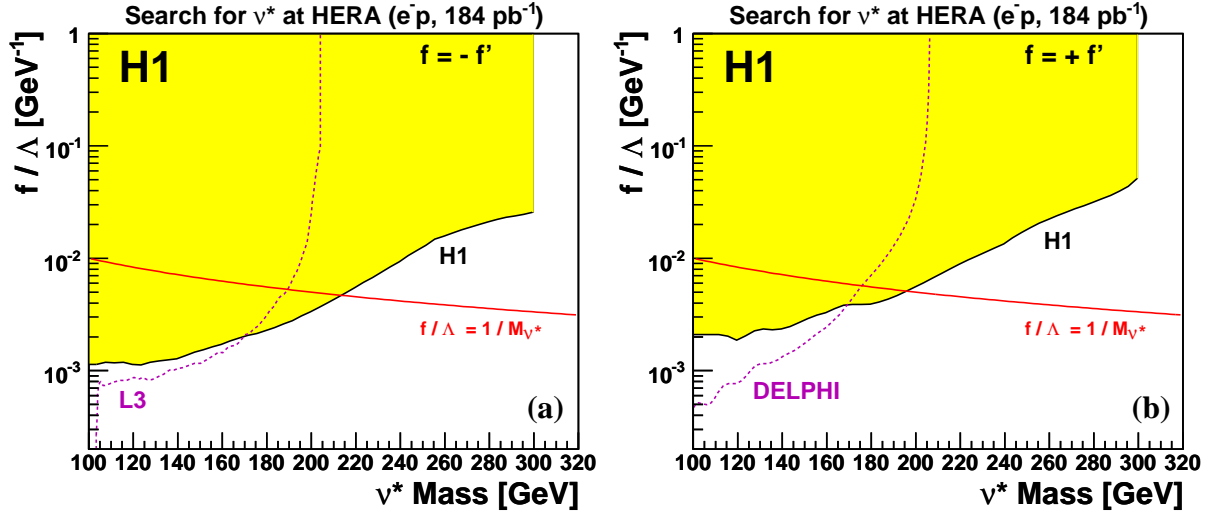


Figure 3: Exclusion limits at 95% CL on the coupling f/Λ as a function of the mass of the excited neutrino with the assumptions (a) $f = -f'$ and (b) $f = +f'$. The excluded domain based on all H1 e^-p data is represented by the shaded area. Values of the couplings above the curves are excluded. The dashed line corresponds to the exclusion limit obtained at LEP by the L3 Collaboration [39] in (a) and by the DELPHI Collaboration [40] in (b).

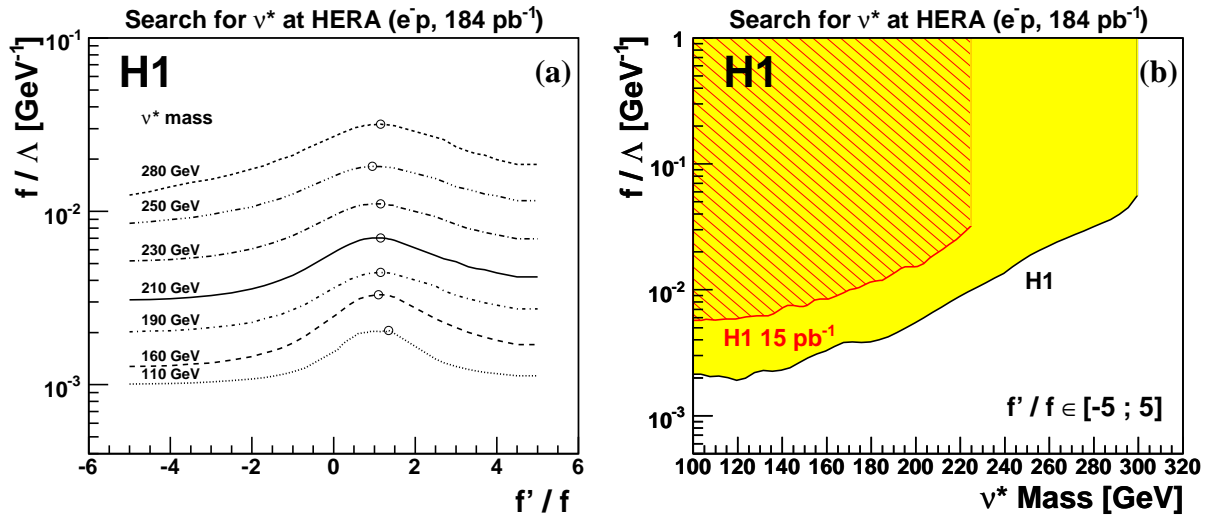


Figure 4: (a) Exclusion limits at 95% CL on the coupling f/Λ as a function of the ratio f'/f . Each curve corresponds to a different ν^* mass. The circle indicates the weakest limit for each mass. (b) Exclusion limit at 95% CL on the coupling f/Λ as a function of the mass of the excited neutrino (shaded area). This limit corresponds to the weakest limit on f/Λ for f'/f values in the interval $[-5; +5]$. The hatched area corresponds to the exclusion domain obtained by H1 in a previous analysis [2]. The regions above the lines are excluded.